



Solar-induced heterogeneous photocatalytic degradation of methyl-paraben



Theodora Velegraki^{a,b,*}, Evroula Hapeshi^{b,c}, Despo Fatta-Kassinou^{b,c}, Ioannis Poullos^a

^a Department of Chemistry, University of Thessaloniki, Thessaloniki 54124, Greece

^b Department of Civil and Environmental Engineering, University of Cyprus, P.O. Box 20537, 1678 Nicosia, Cyprus

^c Nireas, International Water Research Centre, University of Cyprus, P.O. Box 20537, 1678 Nicosia, Cyprus

ARTICLE INFO

Article history:

Received 15 July 2014

Received in revised form 6 November 2014

Accepted 10 November 2014

Available online 18 November 2014

Keywords:

Photocatalysis

Methyl paraben

PCPs

Titanium dioxide

Antimicrobial

ABSTRACT

A solar-induced heterogeneous photocatalytic study on the treatment of methyl-paraben in water has been performed. A solar simulator equipped with a 150 W xenon ozone-free lamp was employed for the experimental runs. Various commercial TiO₂ catalysts have been assessed and the effect of catalyst loading has been extensively studied. Titanium dioxide Aeroxide P-25 was determined as the optimum catalytic material, even at low catalyst loadings. MeP abatement increased with increasing P-25 loading up to 0.5 g L⁻¹, above which further increase brings no actual improvement on the initial rate of the reaction. The addition of an electron acceptor (i.e. hydrogen peroxide) inhibited the degradation rate of MeP, whereas superoxide radicals were found to be the dominant reactive species in the heterogeneous solar-induced photocatalytic degradation of MeP. Experimental design methodology was applied to assess the significance of variables such as initial pH₀, MeP concentration and catalyst dosage and to evaluate their effect on the pseudo-first order reaction rate constant (k_{app}) of the photocatalytic reaction. Complete elimination of 1 mg L⁻¹ MeP was achieved after 35 min at inherent pH 5.2 and 0.5 g L⁻¹ Aeroxide P-25, whereas for the respective run with 10 mg L⁻¹ MeP 240 min reaction time was required. Under the latter conditions, 42% of mineralization was obtained and six intermediates were identified by GC–MS, namely propyl acetate, 2-(2-butoxyethoxy) ethanol, 2,5-dihydroxy-methyl benzoate, hydroquinone, diethyl phthalate and 1,2-benzenedicarboxylic acid bis-(2-methylpropyl) ester.

© 2014 Elsevier B.V. All rights reserved.

1. Introduction

Ever since the first use of parabens as preservatives in drugs around 1920 [1], they are now considered as the most abundant organic substance present in various formulations of Personal Care Products (PCPs) (i.e. facial and body cosmetics, skin and hair care products), where they act as broad-spectrum antimicrobials and anti-fungals to avoid spoilage and thus increase the shelf life [2–4].

Parabens are synthetic esters of *p*-hydroxybenzoic acid, with alkyl substituents ranging from methyl to butyl or benzyl groups [5]. Methyl paraben (MeP) is considered the most utilized antimicrobial amongst a homologous series of parabens (e.g. methyl, ethyl, propyl, butyl, heptyl and benzyl paraben), used either on its own or as a mixture with propyl paraben in order to enhance the antimicrobial performance (i.e. synergistic effect) [6].

* Corresponding author at: Department of Chemistry, University of Thessaloniki, Thessaloniki 54124, Greece. Tel.: +30 2310 997744; fax: +30 2310 997709.

E-mail addresses: thvelegraki@auth.gr, thvelegraki@gmail.com (T. Velegraki).

More than a decade ago, a number of studies reported potential paraben estrogenicity and provided evidence of intact parabens being present in human breast cancer tissue, thus raising serious concerns in regard to human health and environmental safety [7–9]; to appease public concern numerous cosmetics industries decided to voluntarily exclude the use of parabens from their products, thus introducing to the market the so called ‘paraben free’ formulae. To this point, the use of parabens remains a controversial issue and actual connection between the use of paraben-containing underarm cosmetics and breast cancer has not been verified [10].

Notwithstanding the alleged exclusion of parabens from PCPs, recent reports from the Cosmetic Ingredient Review Expert Panel revealed that the number of cosmetics containing parabens was increased by 1.7 times in 2006 compared to 1981 [11]. However, there seems to be a slightly decreasing trend in the paraben content of PCPs; in early 1980s, most formulations contained parabens in concentrations up to 1% or more [1], whereas, a decade later, another study reported that the content of parabens in 215 tested products from the Danish market ranged from 0.01% to 0.87% [3].

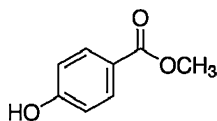


Fig. 1. Physicochemical properties of methyl-paraben.

The widespread use of parabens in PCPs, pharmaceuticals and food products ultimately leads to high levels of human exposure [12,13]; at the same time, studies regarding the activity of parabens as xeno-estrogens continue to emerge [14–18] causing escalating concerns. In European Union (EU) countries, the allowable content of parabens in cosmetic products is 0.4% for single ester and 0.8% for mixtures of all parabens [19]. The same threshold limits have been adopted by the United States (Food and Drug Administration, FDA) and Canada (Health Canada). So far, no legislation exists in country level [20], with the exception of Denmark which in 2011 decided to introduce additional restrictions, banning the use of some parabens (propyl, isopropyl, butyl- and isobutyl-parabens) in personal care products intended for children younger than 3 years [21].

The presence of parabens in wastewater treatment plants (WWTPs) has been confirmed through measurements of intact esters of parabens in raw sewage at levels as high as 2.92 mg L^{-1} and 2.43 mg L^{-1} for methyl and propyl paraben, respectively (i.e. the parabens detected at the highest levels) [22,23]; even though a major source of parabens entering the WWTPs is the washing-off of PCPs prior to skin absorption, however, the presence of intact paraben esters in human urine verifies that these compounds may escape metabolism by either skin esterase if exposure is dermal, or by intestinal and liver metabolic systems if exposure is oral [24].

Despite the considerable removal during conventional sewage treatments that may reach up to 99.9%, parabens have been still detected in ground and/or surface water [25–28].

Up to now, there are some studies that have investigated the elimination of parabens from aqueous matrices with varying process efficacies; photolysis reactions induced by both solar and UVC irradiation resulted in low removal efficiencies [29–31]. Higher removal efficiencies were achieved by coupling UV irradiation with H_2O_2 [32,33] or by applying advanced oxidation processes such as ozonation [34], UV-induced photocatalysis [35,36] and electrochemical oxidation on BDD anode [37].

The present study aims to investigate the TiO_2 -mediated photocatalytic degradation of methyl-paraben (MeP) under the influence of simulated solar light. To the best of our knowledge, this is the first study reporting solar-induced photocatalytic degradation of MeP employing titania catalysts. The influence of various commercial TiO_2 -type catalysts, the catalyst loading, the effect of the water matrix and addition of oxidant (e.g. hydrogen peroxide) on the efficiency of the process was evaluated. Experimental design methodology was applied to assess significant variables and investigate their effect on MeP degradation. The presence of radical scavengers was employed to provide insight on the photo degradation mechanism through different active species. Transformation products of MeP were identified and a degradation pathway was proposed.

2. Materials and methods

2.1. Materials

Methyl-paraben (>99%) was supplied by Fluka and was used as received, protected from any source of light and air and stored at room temperature. The chemical structure and main properties of MeP are shown in Fig. 1.

The photocatalysts used were commercial TiO_2 powders, i.e. the benchmark catalyst Aeroxide P-25 (Evonik Industries, Germany),

Kronos Vlp 7000 and Kronos Vlp 7001 (both from Kronos Titan GmbH, Germany) (Table 1). NaOH and H_2SO_4 were used to adjust the pH when necessary. Hydrogen peroxide (H_2O_2 , 30% w/v) was supplied by Merck and used without further purification. Double distilled water (Millipore Waters Milli-Q) was used for the preparation of all aqueous solutions employed in the present study. HPLC grade acetonitrile was purchased from Merck (Peypin, France), ammonium acetate was supplied by Panreac and MeOH from ChemLab. The wastewater was collected from a municipal wastewater treatment plant (WWTP) downstream of the disinfection unit currently employing chlorination and was characterized as follows: pH 7.5, electrical conductivity $982 \mu\text{S cm}^{-1}$, COD = $6 \text{ mg O}_2 \text{ L}^{-1}$, TSS = 3 mg L^{-1} .

2.2. Experimental setup and procedure

Photocatalytic experiments were carried out in a bench-scale open Pyrex glass reactor (0.3 L capacity) located directly below the beam output of a solar simulator (Newport, model 96000) equipped with a 150 W xenon ozone-free lamp and an Air Mass 1.5 Global Filter (Newport, model 81094) which simulates solar irradiation reaching the surface of the earth at a zenith angle of 48.2° . The output irradiance was measured actinometrically using 2-nitrobenzaldehyde as chemical actinometer and was calculated at 7.5 W m^{-2} [38,39].

All experiments were conducted in a photochemical batch reactor made of borosilicate glass. In a typical experimental run 0.3 L of known concentration of MeP aqueous solution were loaded in the reaction vessel along with an appropriate amount of catalyst. The suspension was left in the dark under continuous magnetic stirring for 30 min to reach equilibrium state. Samples were withdrawn right after equilibrium state between catalyst and substrate had been reached and prior to irradiation. This was considered the time zero of the reaction. Samples were withdrawn at frequent time intervals and were centrifuged at 13,000 rpm for 6 min to remove the catalyst particles. For experimental runs necessitating the use of H_2O_2 as oxidant, a predetermined volume of 30% H_2O_2 was inserted in the reaction medium before turning on the lamp. In order to eliminate any residual hydrogen peroxide remaining in the sample aliquots a small amount of Na_2SO_3 solution was added and the oxidant elimination was verified with Merckquant® test strips.

2.3. Methodology

2.3.1. Analytical determinations

The decay of MeP concentration during the reaction was monitored through a high performance liquid chromatography and mass spectrometry (HPLC–MS) system in negative ionization mode. Analysis was carried out using a Waters Alliance 2695 HPLC system coupled to a benchtop triple quadrupole Quattro micro MS from Waters – Micromass (Manchester, UK) equipped with an electrospray probe and a Z-spray interface. Chromatographic separation was achieved on a Luna C-18 column ($5 \mu\text{m}$, $250 \text{ mm} \times 4.6 \text{ mm}$) and a security guard column ($4 \text{ mm} \times 3 \text{ mm}$), both from Phenomenex. The mobile phase eluted isocratically for 7 min with acetonitrile (50%) – ammonium acetate 5 mM (50%) at 30°C , while the injection volume was $50 \mu\text{L}$. The flow rate was 1 mL min^{-1} ; however, the flow was split and reduced to 0.4 mL min^{-1} before entering the mass spectrometer. MS detection was achieved in SIR (Selected Ion Recording) mode (m/z 151).

Mineralization was followed by measuring the dissolved organic carbon (DOC) by direct injection of filtered samples into a Shimadzu VCSH Total Organic Carbon Analyzer and pH was determined with a Crison GLP 21 pH meter. Residual hydrogen peroxide was measured

Table 1
Characteristics of TiO₂ photocatalysts used in the present study.

| | P-25 | Kronos Vlp 7000 | Kronos Vlp 7001 |
|-----------------------------------|----------------------------------------|-------------------------------------|-------------------------------------|
| Appearance (form) | White powder | Pale beige powder | Pale beige powder |
| TiO ₂ content (purity) | 99.5% | 95% | 95% |
| Composition | 70% anatase, 30% rutile | >85% anatase | >85% anatase |
| Specific surface area (BET) | 55 ± 15 m ² g ⁻¹ | >225 m ² g ⁻¹ | >225 m ² g ⁻¹ |
| Crystallite size | 21 nm | 15 nm | 15 nm |

with colorimetric determination with Mercquant[®] Peroxide test strips.

2.3.2. Toxicity evaluation

Toxicity assessment was performed according to the commercially available Artoxkit MTM, which is based on the observation of *Artemia franciscana* immobilization after 24 h of exposure to the treated samples. A control test was performed using simulated seawater. The tests were carried out in three replicates for each sample to ensure repeatability and minimize experimental errors. *A. franciscana* in the form of dehydrated cysts was obtained commercially from a pet supply shop (Sera[®] Artemia-mix). Prior to use, the bag contents (i.e. Artemia cysts and sodium chloride) were introduced in 500 mL aerated deionized water and were hatched into nauplii larvae after 24 h at 29 °C under constant lighting (min. 3000–4000 lx) and aeration. Sample salinity was corrected to 2.75% and dilutions were made with standard sea water medium (i.e. 2.75% salinity) prepared and stored at 4 °C. *Artemia* nauplii (<30 h old) were exposed to untreated and treated samples in triplicate to score frequencies of immobilization of 10 nauplii in 1 mL volumes. The incubation period took place in the dark at 25 °C and after 24 h the immobilized nauplii were measured.

2.3.3. Solid phase extraction (SPE)

In order to pre-concentrate the samples and identify the intermediates formed during photocatalytic degradation, the filtered suspensions were subjected to solid phase extraction. The filtered suspensions at different irradiant time intervals were extracted using 3 mL cartridges packed with 200 mg ISOLUTE ENV+ (BIO-TAGE). The cartridges were pre-conditioned with 5 mL methanol followed by 5 mL acidified water (pH 2.6, H₃PO₄) at a flow rate of 1 mL min⁻¹ using a Varian vacuum manifold. Subsequently, 25 mL acidified sample (pH 2.6) were passed through the cartridge at a flow rate of 2 mL min⁻¹. SPE cartridge was dried for 10 min under N₂ stream. The analytes were then eluted using two aliquots of 1 mL methanol at a flow rate of 2 mL min⁻¹. The extracts were dried under N₂ stream and re-dissolved in 100 µL MeOH. Aliquots of 1 µL were injected into GC–MS for further analysis.

2.3.4. Identification of intermediates with gas chromatography–mass spectrometry

Gas chromatographic analysis for by-products identification was carried out on a Shimadzu QP5050 GC–MS system (Tokyo, Japan). The analytical column was DB-5MS + DG, 30 m + 10 m Duraguard, 0.25 mm I.D., 0.25 µm film thickness (J&W Scientific). Injections were performed in the splitless mode, the mass spectrometer was used in the electron impact mode (70 eV, *m/z* 40–300 amu) and the carrier gas (helium) flow was at 1.3 mL min⁻¹. The interface temperature was set at 270 °C. The temperature program of the GC was from 35 °C (2 min) to 260 °C (2 min) at 10 °C min⁻¹. The injector temperature was set at 250 °C.

2.4. Experimental design

The selection of the optimum experimental conditions for the photocatalytic degradation of MeP was based on an experimental

design approach; a full factorial design, consisting of 11 experiments, was composed, to assess the effect of three independent variables assuming two values or levels (i.e. low and high). The variables considered for the study were the initial concentrations of MeP, the amount of catalyst P-25 and initial pH (Table 2). The pseudo-first order reaction rate constant (*k*_{app}) calculated for the first 15 min of reaction was considered as the response factor.

3. Results and discussion

3.1. Effect of catalyst amount

The photocatalytic degradation of MeP at inherent pH (i.e. 5.2) was investigated for different catalyst loadings using the three commercially available TiO₂ catalysts (Fig. 2(a)–(c)). Preliminary experiments performed in the absence of catalyst (i.e. photolysis) verified the high photochemical stability of MeP under simulated solar light at inherent pH (data not shown). In addition, adsorption of MeP onto catalyst surface was found to be negligible (i.e. less than 3%) for all three catalysts under investigation (Fig. 2(a)–(c)).

It is worth noting, that although both carbon-doped Kronos catalysts (i.e. Kronos Vlp 7000 and Kronos Vlp 7001) are considered highly active under visible irradiation, whereas P-25 is mainly activated under UV light, the superiority of P-25 is evident (Fig. 2(c)); P-25 loadings ranging from 0.1 to 1 g L⁻¹ lead to complete elimination of MeP within 35–45 min of solar irradiation, whereas Kronos Vlp 7000 and Kronos Vlp 7001 reached merely 9–42% and 7–21% degradation, respectively, after 45 min with catalyst amounts ranging from 0.1 to 1 g L⁻¹ (Fig. 2(a) and (b)). P-25 has the smallest surface area and different composition from the other TiO₂ powders (Table 1); however, the higher efficacy of P-25 on MeP elimination compared with the respective efficacies of Kronos Vlp 7000 and Kronos Vlp 7001 can be attributed to (i) the existence of the interface between the two crystalline phases (i.e. anatase and rutile) which promotes the generation of active sites for photocatalytic activity [40,41] and (ii) the ‘quantum size effect’, i.e. when the particles become too small, there is a ‘blue shift’ with an increase of the band gap energy, detrimental to the near UV-photon absorption, and an increase of the electron–hole recombination [42].

Fig. 2(c) shows that the photocatalytic degradation of MeP increases with increasing P-25 loading from 0.01 to 0.5 g L⁻¹, while further increase leads to no actual improvement in the degradation rate. This is also evident from Fig. 3, where the effect of P-25 catalyst loading on the initial reaction rate *r*₀ is presented along with the respective regression coefficients (Table 3). The pseudo-first order reaction rate practically reaches a plateau above a certain catalyst

Table 2
Variable levels in a 2³ full experimental design.

| Variable | Coded variable level | |
|------------------------------------------|----------------------|-----------|
| | Low (–1) | High (+1) |
| [MeP] ₀ (mg L ⁻¹) | 1 | 10 |
| [P-25] (g L ⁻¹) | 0.1 | 0.5 |
| pH ₀ | 5.2 | 9.2 |

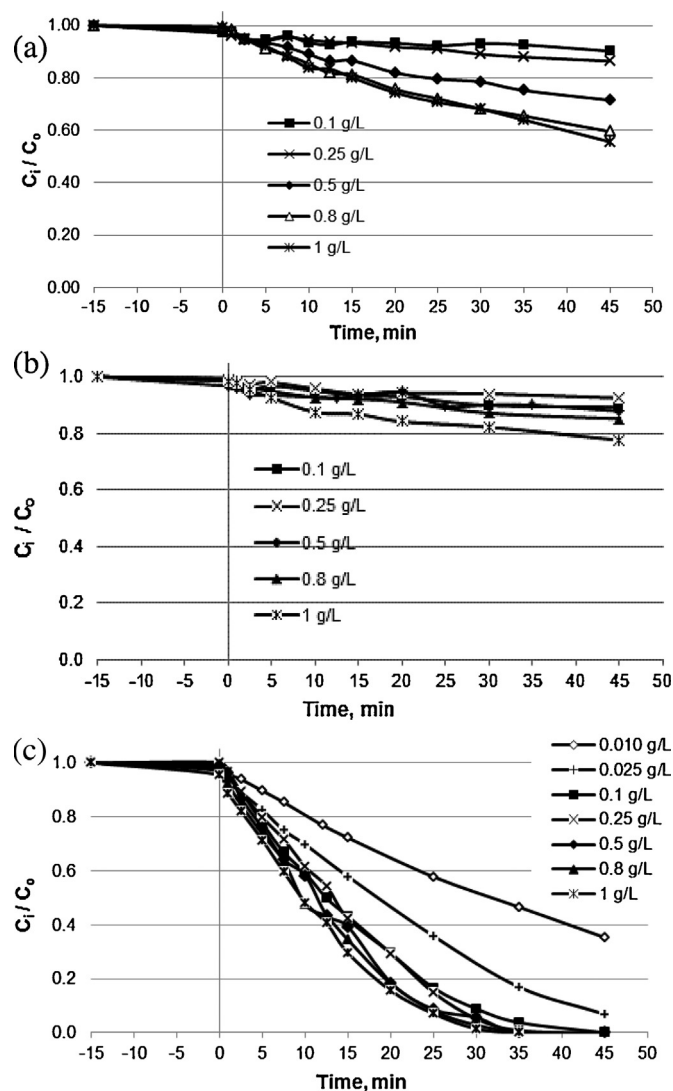


Fig. 2. Effect of catalyst loading on solar photocatalytic degradation of MeP employing different TiO₂ catalysts: (a) Kronos Vlp 7000, (b) Kronos Vlp 7001 and (c) P-25 Evonik. Inherent pH 5.2; [MeP]₀ = 0.001 g L⁻¹.

loading (i.e. the point where the reaction rate becomes independent of the catalyst loading) which is at 0.5 g L⁻¹ P-25.

As the catalyst particles in the reaction medium increase, so does the number of active sites available for photon absorption; however, once a threshold loading value has been reached and

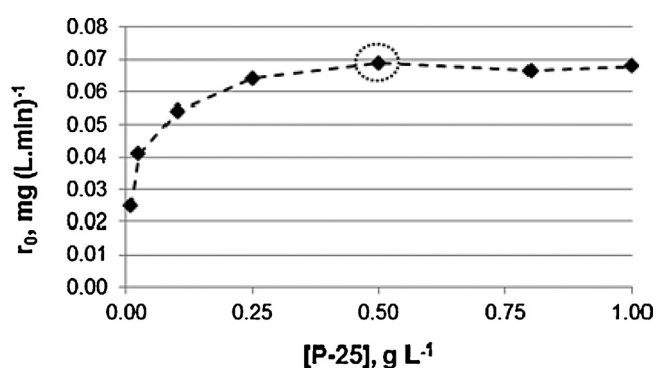


Fig. 3. Effect of P-25 catalyst loading on the initial reaction rate r_0 of heterogeneous photocatalytic oxidation of MeP. Inherent pH 5.2; [MeP]₀ = 0.001 g L⁻¹.

Table 3

Pseudo-first order kinetic rate constants (k_{app}) and initial reaction rate r_0 for MeP degradation at different catalyst loadings and respective regression coefficients (R^2).

| [P-25] (g L ⁻¹) | k_{app} ^a (min ⁻¹) | R^2 | r_0 (mg (L min) ⁻¹) |
|-----------------------------|---------------------------------------------|--------|-----------------------------------|
| 0.010 | 0.0217 | 0.9953 | 0.0249 |
| 0.025 | 0.0350 | 0.9971 | 0.0409 |
| 0.100 | 0.0516 | 0.9918 | 0.0541 |
| 0.250 | 0.0602 | 0.9795 | 0.0641 |
| 0.500 | 0.0595 | 0.9766 | 0.0689 |
| 0.800 | 0.0658 | 0.9843 | 0.0665 |
| 1.000 | 0.0668 | 0.9946 | 0.0678 |

^a Calculated for the first 15 min of the reaction.

exceeded, scattering and screening phenomena commence, thus resulting in non-uniform light intensity distribution [43–45].

The Langmuir–Hinshelwood (L–H) model is often used to describe the solid–liquid reactions occurring in heterogeneous semiconductor photocatalysis (Eq. (1)), where r is the reaction rate, k_{LH} is the apparent L–H rate constant, θ is the surface coverage of the pollutant, K_L is the Langmuir adsorption constant taking into account several parameters (i.e. the catalyst's mass, efficient photon flow, O₂ layer, etc.) [46] and C_{eq} is the equilibrium concentration of the substrate. According to Herrmann [47] it can be assumed that at highly diluted solutions of the organic substrate (i.e. $C < 10^{-3}$ mol L⁻¹) the $K_L C_{eq} \ll 1$, thus the denominator of Eq. (1) can be neglected which ultimately leads to the simplified expression of Eq. (2), where k_{app} is the apparent rate constant of a pseudo first order reaction:

$$r = -\frac{dC}{dt} = k\theta = k_{LH} \frac{K_L C_{eq}}{1 + K_L C_{eq}} \quad (1)$$

$$r = -\frac{dC}{dt} = k_{LH} K_L C_{eq} = k_{app} C_{eq} \quad (2)$$

$$\ln \frac{C_{eq}}{C} = k_{app} t \quad (3)$$

Integrating Eq. (2) leads to Eq. (3). By plotting $\ln(C_{eq}/C)$ versus t , the apparent rate constant (k_{app}) can be obtained from the slope of the curve obtained. The plot $\ln(C_{eq}/C)$ versus t for P-25 concentration 0.01 g L⁻¹, 0.025 g L⁻¹, 0.1 g L⁻¹, 0.25 g L⁻¹, 0.5 g L⁻¹, 0.8 g L⁻¹ and 1 g L⁻¹ describes a linear behavior with the respective linear regression coefficients shown in Table 3.

3.2. Effect of oxidant addition

It is widely accepted that the addition of an oxidant acting as electron acceptor is expected to accelerate the heterogeneous photocatalytic degradation by suppressing the recombination of electrons (e_{cb}^-) and holes (h_{vb}^+) through e_{cb}^- trapping or by inducing the formation of superoxide radical anions (O₂^{•-}) which in turn produces hydroxyl radicals ($\cdot OH$) [48–51]. In an attempt to assess the influence of an electron acceptor (i.e. hydrogen peroxide) in TiO₂-mediated photocatalytic degradation of 0.001 g L⁻¹ MeP, the addition of varying concentrations of H₂O₂ has been investigated.

In the absence of catalyst the addition of 10–75 mg L⁻¹ H₂O₂ (i.e. corresponding to about 2.5-fold and 20-fold, respectively, the stoichiometric amount for complete oxidation of 0.001 g L⁻¹ MeP with hydrogen peroxide) into the solar-irradiated aqueous solution brings about 15–48% MeP degradation, respectively (Fig. 4). Bearing in mind that (i) direct photolysis of MeP does not occur under the present experimental conditions and (b) semi-quantitative measurements showed that H₂O₂ is consumed during reaction (data not shown), it can be concluded that the observed abatement of MeP is owed to direct H₂O₂ photodecomposition by solar irradiation and generation of hydroxyl radicals [48,52].

In the presence of 0.5 g L⁻¹ Kronos Vlp powders, the introduction of varying amounts of H₂O₂ ranging from 3.8 mg L⁻¹ (i.e.

Table 4MeP elimination after 45 min of H₂O₂-assisted solar photocatalytic degradation employing 0.5 g L⁻¹ Kronos Vlp 7000 and Kronos Vlp 7001 catalysts.

| Catalyst | 3.8 mg L ⁻¹ H ₂ O ₂ | 10 mg L ⁻¹ H ₂ O ₂ | 25 mg L ⁻¹ H ₂ O ₂ | 75 mg L ⁻¹ H ₂ O ₂ |
|-----------------|------------------------------------------------------|-----------------------------------------------------|-----------------------------------------------------|-----------------------------------------------------|
| Kronos Vlp 7000 | 47% | 50% | 53% | 57% |
| Kronos Vlp 7001 | 18% | 32% | 48% | 62% |
| No catalyst | nd | 15% | 30% | 48% |

nd, not determined.

equivalent to 1.14 mg H₂O₂ which is the stoichiometric amount required for 1 mg L⁻¹ MeP oxidation) up to 75 mg L⁻¹ seems to improve the removal percentage of MeP after 45 min (Table 4); that is, for Kronos Vlp 7000 and Kronos Vlp 7001, the process efficacy increased from 47% to 57% and from 18% to 62%, respectively. The respective experimental runs without H₂O₂ shown in Fig. 2(a) and (b) reached barely 26% (Kronos Vlp 7000) and 9% (Kronos Vlp 7001) after 45 min. These findings underline the role of H₂O₂ as a promoter during solar-induced MeP photocatalytic degradation employing Kronos Vlp 7000 and 7001 powders. The observed enhancing effect can be owed to several reasons; firstly, the H₂O₂ molecules scavenge TiO₂ surface-trapped electrons, thus limiting the electron-hole recombination rate and increasing the efficiency of hole utilization (i.e. direct oxidation of organic pollutants); secondly, the photo-induced splitting of H₂O₂ that leads to the production of hydroxyl radicals; and thirdly, the alternative role of H₂O₂ as source of oxygen in the reaction system that could be oxygen-deficient at some point during the process.

Notwithstanding, this promoting effect is not corroborated in the case of the respective runs with 0.5 g L⁻¹ P-25; in the latter case, the addition of H₂O₂ in concentrations ranging from 3.8 to 75 mg L⁻¹ clearly inhibits the reaction rate of the photocatalytic degradation of MeP (Fig. 4). This discrepancy amongst Kronos Vlp catalysts and P-25 could be due to differences in the BET surface, impurities, lattice mismatches or density of hydroxyl groups present on the catalyst's surface (Table 1) that could affect the adsorption behavior of degradation intermediates and the lifetime and recombination rate of electron-hole pair. With these in mind, the dominant reactive species may vary depending on the type of TiO₂ particles employed, thus leading toward different reaction mechanisms. The inhibiting effect of H₂O₂ that is presently reported may be attributed to the scavenging effect of hydroxyl radicals by hydrogen peroxide and/or modification of the P-25 surface by H₂O₂ adsorption; that is, H₂O₂ may compete with MeP for the active sites onto TiO₂ P-25 particles which ultimately leads to lower efficiency for MeP photocatalytic degradation [53–55]. In addition, under air-equilibrated conditions, dissolved oxygen may also act as an electron scavenger yielding superoxide radical anions

(R1) which, in turn, react with protons (generated by valence band holes reacting with water) to form peroxide radicals (R2) [56].

Assuming that the aforementioned reactive species contribute significantly to the overall degradation rate, the addition of H₂O₂ would act competitively for the formation of superoxide and peroxide radicals through reaction R3, which prevents the recombination of electron/hole pairs. This assumption is further discussed in the following section:



3.3. Effect of matrix

The heterogeneous TiO₂-mediated photocatalytic process is based on the generation of highly reactive oxidative species (ROS) such as hydroxyl radicals (HO[•]), superoxide radicals (O₂^{•-}) and valence band holes (h_{vb}⁺) which can undergo redox reactions with most persistent organic compounds. In this context, an estimation of the participation of the different reactive species has been attempted, so as to gain a deeper insight of the photocatalytic mechanism of MeP degradation in the presence of 0.5 g L⁻¹ P-25. Three different radical scavengers have been chosen, i.e. 1,4-benzoquinone, potassium iodide and iso-propanol. 1,4-Benzoquinone selectively quenches O₂^{•-}, potassium iodide reacts with both h_{vb}⁺ and HO[•] and iso-propanol is known to be an efficient HO[•] scavenger. The effect of the addition of radical scavengers on MeP degradation is presented in Fig. 5. It is observed that the addition of potassium iodide and iso-propanol at 5 mM caused an inhibition in MeP degradation from 100% to 65% and 21%, respectively, after 35 min. The greater inhibition of the reaction through iso-propanol compared to potassium iodide provides an indication that HO[•] play a more important role in the photocatalytic degradation of MeP than h_{vb}⁺ [57,58]. Similarly, with the addition of 5 mM 1,4-benzoquinone, MeP degradation was strongly suppressed, which suggests the predominance of O₂^{•-} as reactive species during the solar-induced photocatalytic degradation of MeP with P-25 [59]. These findings verify the assumption made in the previous section that the addition of hydrogen peroxide

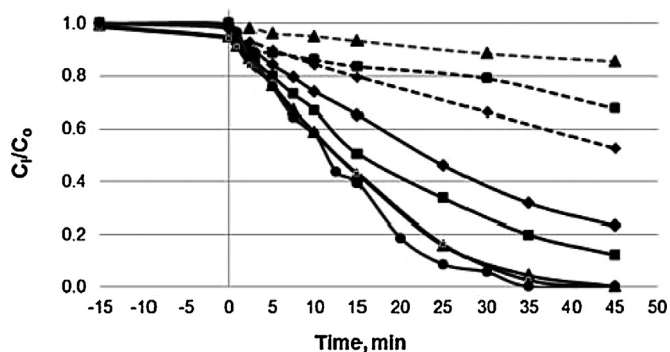


Fig. 4. Effect of H₂O₂ addition in varying concentrations on P-25 TiO₂-mediated solar photocatalytic degradation of MeP. (●) 75 mg L⁻¹ H₂O₂; (■) 25 mg L⁻¹ H₂O₂; (▲) 10 mg L⁻¹ H₂O₂; (x) 3.8 mg L⁻¹ H₂O₂; (●) only P25; dashed lines represent runs without TiO₂, whereas solid lines represent the corresponding runs with H₂O₂ and TiO₂. Inherent pH 5.2; [MeP]₀ = 0.001 g L⁻¹; [P-25] = 0.5 g L⁻¹.

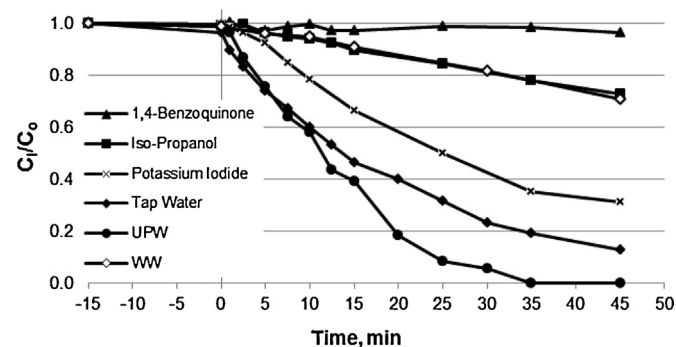
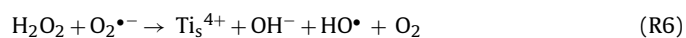


Fig. 5. Effect of matrix and radical scavenger on TiO₂-mediated solar photocatalytic degradation of MeP. Inherent pH 5.2; [MeP]₀ = 0.001 g L⁻¹; [P-25] = 0.5 g L⁻¹; [radical scavenger] = 5 mM.

inhibits the degradation rate as it competes with oxygen for electrons (reactions R1 and R3) thus limiting the formation of $O_2^{\bullet-}$ radicals. Salvador et al. [60] reported that the only route for generation of free HO^{\bullet} in the water layer close to the TiO_2 surface is via the electro-reduction of dissolved oxygen with photogenerated conduction band electrons (reactions R1–R2 and R4–R6), since the photo-oxidation of non-adsorbed water molecules or solvated hydroxyl groups with free $h_{\nu b}^+$ is hindered both thermodynamically and kinetically.



In an attempt to evaluate the effect of the water matrix on MeP photocatalytic degradation, the respective experimental run was conducted employing two different aqueous matrices, i.e. tap water and wastewater (WW). As is evident from Fig. 5, the degradation efficiency decreases as the complexity of the water matrix increases; water components like calcium, magnesium, iron, zinc, copper, bicarbonate, phosphate, nitrate, sulfate, chloride, and dissolved organic matter can affect the photocatalytic degradation rate of organic pollutants since they can be adsorbed onto the surface of TiO_2 or even act as radical scavengers toward the formation of their respective radicals, whose oxidation potential is lower than that of hydroxyl radicals HO^{\bullet} [61]. For instance, the 35 min MeP abatement is 100%, 80% and 20% in UPW, tap water and WW, respectively. The discrepancies in process efficacy observed for wastewater and tap water can be attributed to the fact that wastewater has a much more complex matrix than tap water; in this context, the oxidizing agents are competitively consumed in reactions involving the organic matter present in treated wastewater.

3.4. Assessment of experimental variables

The design consisted of two series of experiments: (i) a 2^k factorial design (where $k = 3$ variables), resulting in eight experiments with all possible combinations of the coded variables and (ii) three replicates at the center point (0, 0) of the design (coded value 0). The experimental design matrix, actual levels and response factor values are shown in Table 5.

The following semi-empirical expression in Eq. (4) was obtained from statistical analysis using the software MINITAB at 95% confidence level ($p < 0.05$):

$$Y = 0.0890813 + 0.227903A - 0.00835111B - 0.00895625C - 0.0216778AB - 0.0237153AC + 0.000825BC + 0.00227778ABC \quad (4)$$

where Y refers to k_{app} (min^{-1}) and A , B and C represent the uncoded values of P-25 concentration, MeP concentration [MeP] and pH_0 , respectively.

The model of Eq. (4) consists of first order terms in all possible combinations; the goodness-of-fit was verified by the high correlation coefficient ($R^2 = 94.4\%$), which indicates that 94.4% of the response variability could be explained by the model; similarly, the adjusted determination coefficient $R^2 = 81.4\%$ was also high indicating that the obtained model was significant.

Fig. 6 presents the Pareto chart of the standardized effects to determine the magnitude and the importance of each variable. The chart displays the absolute value of the effects and draws a reference line on the chart, with any effect extending past this line being potentially important; in this context, the initial concentration of MeP, the initial pH_0 and the interaction between [MeP] and pH_0 are all presented as statistically important terms, whereas the

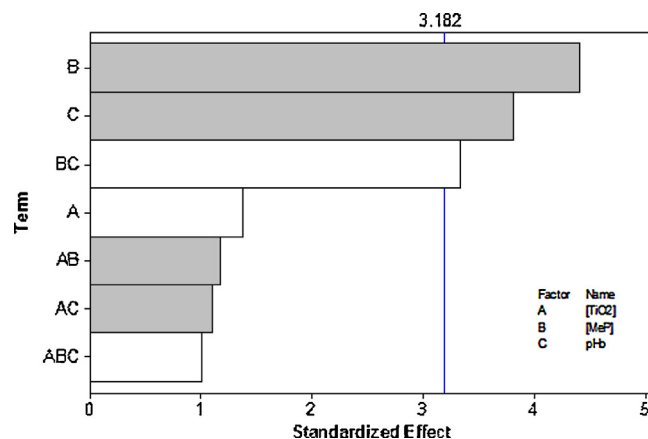


Fig. 6. Standardized effects of single and interaction factors on the pseudo-first order reaction rate constant (k_{app}). Gray bars: negative effect, white bars: positive effect.

catalyst amount and the remaining interaction effects are less significant statistically within the range they are studied and may be explained as random noise. Both the initial substrate concentration and the initial pH show a negative effect in regards to the k_{app} ; that is, the higher the value of each of these two terms within the studied range, the lower the k_{app} of the reaction which in turn signifies lower initial reaction rates.

Fig. 7(a) shows the main effects plot for the important variables, i.e. [MeP] and pH_0 which compares the magnitudes of the main effects and shows in what way the variation of the influential

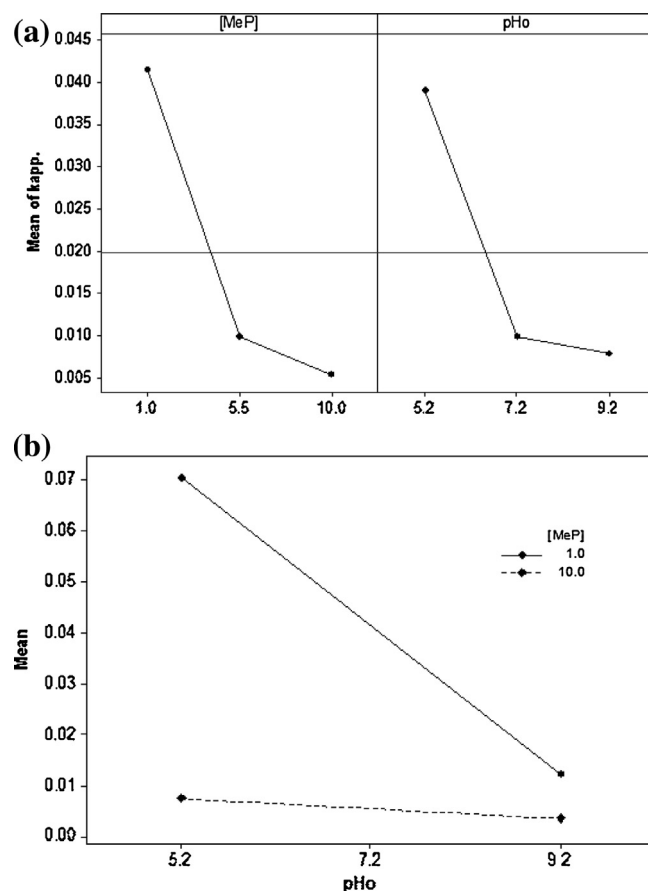


Fig. 7. (a) Main effects plot and (b) interaction plot for pseudo-first order constant (k_{app}) of MeP solar-induced heterogeneous photocatalytic degradation.

Table 5

Full factorial design with actual and coded levels and response factor values.

| Experimental series | Actual (and coded) levels of variables | | | Response factor | |
|------------------------------------|------------------------------------------|-----------------------------|-----------------|---------------------------------------|----------------|
| | [MeP] ₀ (mg L ⁻¹) | [P-25] (g L ⁻¹) | pH ₀ | k _{app} (min ⁻¹) | R ² |
| 2 ³ experimental design | 1 (−1) | 0.1 (−1) | 5.2 (−1) | 0.0516 | 0.9918 |
| | 1 (−1) | 0.5 (+1) | 5.2 (−1) | 0.0895 | 0.9766 |
| | 10 (+1) | 0.5 (+1) | 5.2 (−1) | 0.0087 | 0.9964 |
| | 10 (+1) | 0.5 (+1) | 9.2 (+1) | 0.004 | 0.9927 |
| | 1 (−1) | 0.5 (+1) | 9.2 (+1) | 0.0141 | 0.9945 |
| | 10 (+1) | 0.1 (−1) | 5.2 (−1) | 0.0062 | 0.9906 |
| | 10 (+1) | 0.1 (−1) | 9.2 (+1) | 0.003 | 0.9842 |
| | 1 (−1) | 0.1 (−1) | 9.2 (+1) | 0.0105 | 0.9778 |
| | 5.5 (0) | 0.3 (0) | 7.2 (0) | 0.0104 | 0.9895 |
| Center runs | 5.5 (0) | 0.3 (0) | 7.2 (0) | 0.0105 | 0.9778 |
| | 5.5 (0) | 0.3 (0) | 7.2 (0) | 0.009 | 0.9872 |

variables chosen for photocatalytic MeP elimination affect the response factor. The influence of the single factors considered is depicted wherein the lines indicate the estimated change in k_{app} as each factor moves from its low level to its high level, while maintaining the remaining factor constant at a midway value codified as value 0, between its low and high value. It can be seen that both the initial MeP concentration and pH₀ have similar effects on k_{app} ; increasing the initial concentration of MeP ([MeP]₀) and the initial pH₀ of the solution, results in a decrease in the pseudo-first order reaction rate constant k_{app} . Higher substrate concentration means that the increased number of MeP molecules tends to occupy more catalyst active sites, which in turn hampers the generation of the oxidants [62].

The plot shows that k_{app} increases substantially when pH₀ moves from its center level (i.e. 7.2) toward its low level (i.e. 5.2). This means that higher reaction rates can be attained at acidic pH rather than maintaining the solution between neutral and alkaline conditions. It is well known that variations in the pH value of an aqueous reaction system can be associated with many changes on the process efficacy brought on by modifications of catalyst surface charge, amount of HO· produced, ionization state of the pollutant or even deactivation of the catalyst particles due to poisoning [63]. The isoelectric point (IEP) of TiO₂ Degussa P-25 is ca. 6.5, above and below which the TiO₂ surface becomes negatively and positively charged, respectively. The pK_a of MeP is 8.17 which means that at pH 5.2 – and near neutral, i.e. pH 7.2 – MeP exists mainly in its molecular form and there is no electrostatic attraction with the positively – or negatively – charged TiO₂ particles; this is corroborated by the low adsorption efficiency shown in Fig. 2(c). Likewise, at pH 9.2 MeP exists partly in its ionic form (i.e. the hydroxyl group is deprotonated), whereas the TiO₂ is negatively charged; this facilitates an electrostatic repulsion between the pollutant and the catalyst particles which is verified by very low adsorption capacity (data not shown). Since MeP adsorption onto catalyst is not favored at either acidic or alkaline conditions, its degradation appears to proceed via reactions with reactive radicals in the liquid bulk. The low degradation rate observed at alkaline pH leads to the consideration that hydroxyl radicals may not contribute significantly to MeP oxidation, as it would be expected at increased production of hydroxyl anions [64]. In addition, there are other effects that involve the equilibrium of water dissociation which, in turn, affect the hydroxyl radicals' generation and the oxidative power of the photo-generated holes. However, it is not easy to assess the role of each of these effects. In this context, the higher degradation rates observed at acidic pH can be attributed to the combined activity of different reactive species, i.e. superoxide radicals, hydroxyl radical and photo-generated holes that are favored at acidic conditions, whereas at neutral and alkaline conditions hydroxyl radicals become the dominant species [65].

The interaction plot in Fig. 7(b) shows that the variation in k_{app} is highly pronounced at low [MeP]₀ (i.e. 1 mg L⁻¹) as the pH₀ shifts from 5.2 to 9.2; in contrast, at high MeP concentration (i.e. 10 mg L⁻¹) the respective change is only marginal, which means that pH₀ becomes important at low MeP concentrations.

3.5. Toxicity evaluation

Toxicity assessment was performed during solar-induced heterogeneous photocatalytic degradation of MeP at 0.01 g L⁻¹, pH₀ 5.2 and 0.5 g L⁻¹ P-25; complete elimination of MeP was achieved after 240 min of reaction (data not shown). It was found that the parent compound exhibited very low toxicity to *Artemia nauplii* after 24 h of exposure (i.e. the immobilization was less than 3%), depicting similar measurements to the control (ca. 1% immobilization) (data not shown). The toxicity evolution at different stages of MeP photocatalytic degradation ranging from 0% up to 100% MeP abatement is presented in Fig. 8. It can be observed that toxicity reaches its highest value (i.e. 10% immobilization) at 39% MeP degradation with the corresponding TOC reduction at 20%; further elimination of MeP up to 86%, corresponding to 30% TOC abatement, maintains the toxicity values at slightly higher levels than the untreated solution; these results indicate that the MeP degradation intermediates are potentially more toxic than the parent molecule. Toxicity is reduced after complete elimination of MeP (i.e. after 240 min), even if almost 60% of TOC is still present, which suggests that the intermediates responsible for the toxicity increase have been eliminated with treatment. MeP has been reported to exhibit low eco-toxicity with EC₅₀ ranging between 32 and 62 mg L⁻¹ when *Daphnia magna* was

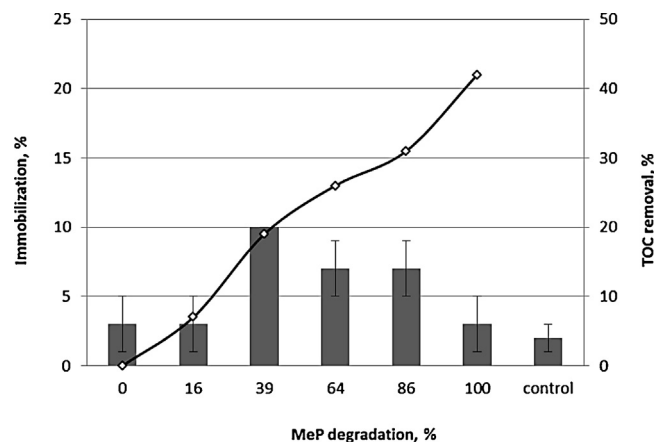
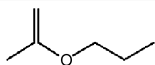
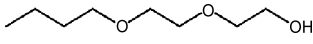

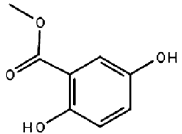
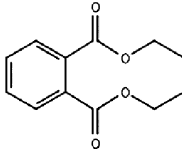
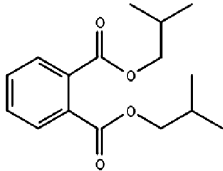


Fig. 8. *Artemia franciscana* nauplii toxicity evolution (bars) and TOC removal (line) during solar-induced heterogeneous photocatalytic degradation of 10 mg L⁻¹ MeP at pH 5.2 and 0.5 g L⁻¹ P-25.

Table 6

Degradation products of MeP identified by GC–MS following solar-induced heterogeneous photocatalysis.

| No | Intermediates (retention time) | Molecular structure | MW (g mol ⁻¹) |
|----|---------------------------------------------------------------------|------------------------------------------------------------------------------------|---------------------------|
| 1 | <i>n</i> -Propyl acetate (4.3 min) |  | 102.1 |
| 2 | 2-(2-Butoxyethoxy) ethanol (11.6 min) |  | 162.2 |
| 3 | Hydroquinone (13.7) |  | 110.1 |
| 4 | 2,5-Dihydroxy-methyl benzoate (16.9 min) |  | 168.1 |
| 5 | Diethyl phthalate (17.3 min) |  | 222.2 |
| 6 | 1,2-Benzenedicarboxylic acid, bis (2-methylpropyl) ester (20.5 min) |  | 278.3 |

used as test microorganism, whereas *Vibrio fischeri* was more sensitive after 15 min of exposure with EC₅₀ measured at 5.9–9.6 mg L⁻¹ [66,67]. On the other hand, chlorinated derivatives of MeP have shown toxicity values that were up to fourfold of those of their parent compound [66].

3.6. Major by-products of methyl-paraben and reaction pathway

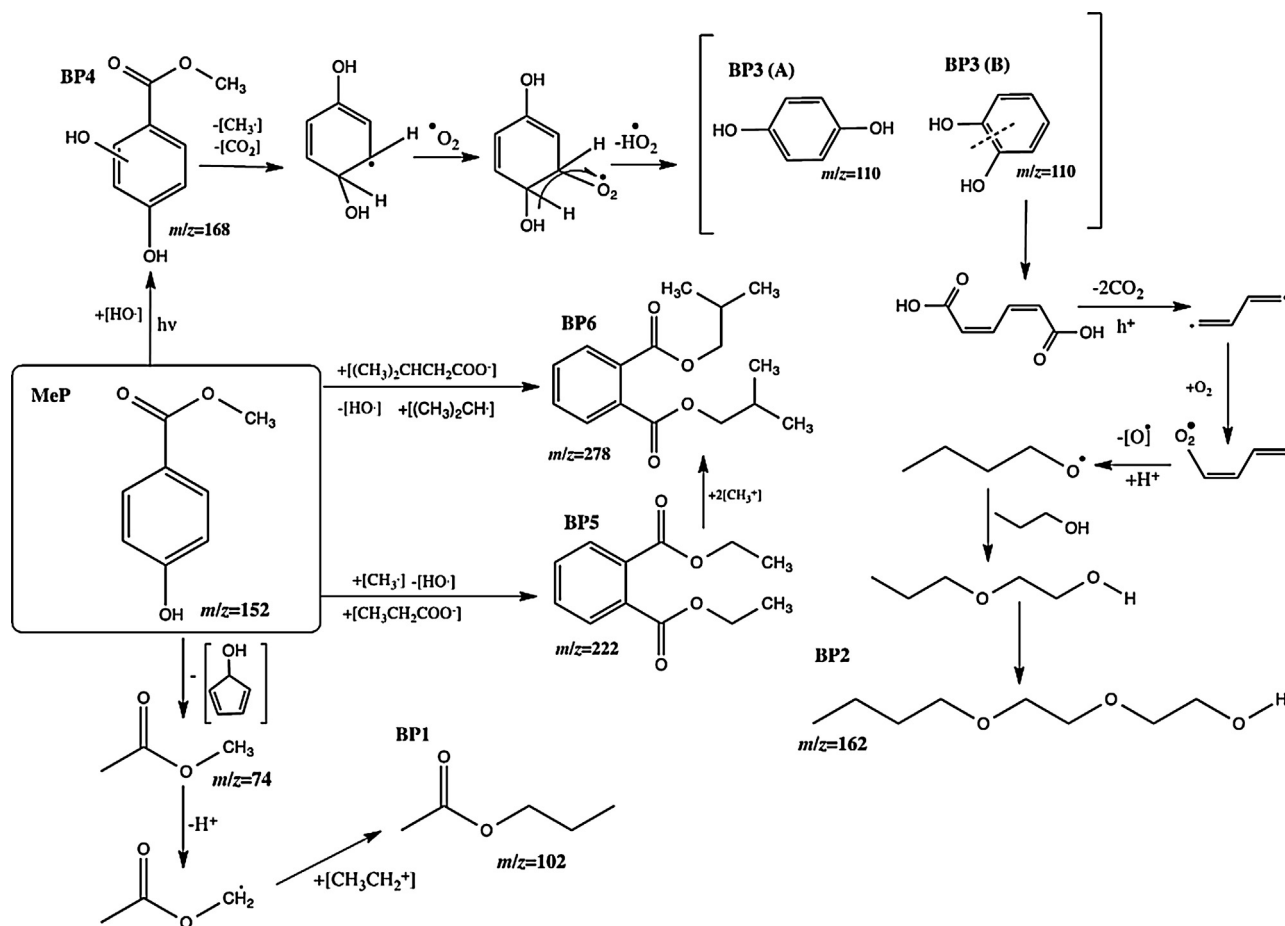
In order to characterize photocatalytic intermediates solar irradiation experiments were carried out at optimal conditions (0.5 g L⁻¹ P-25, inherent pH 5.2) using directly stock MeP solution (0.1 g L⁻¹). Samples were withdrawn at 240 and 360 min of reaction and were pre-concentrated through SPE procedure. In turn, they were analyzed by GC–MS to identify as many intermediates as possible. Identical intermediates were formed during both reaction times and Table 6 summarizes those that were identified by the MS Search software for over 90% similarity as possible degradation products of MeP, along with their GC–MS retention times, molecular weights (MW) and chemical structures.

In the present study, an attempt was made to elucidate the reaction pathways and mechanisms through the identification of by-products (BPs), formed during the photocatalytic treatment procedure of MeP. Scheme 1 illustrates the postulated chemical structures and the exact mass values of the detected ions for the degradation products identified, during the MeP photocatalytic process. Overall, the screening of the treated samples allowed to tentatively identify the formation of six BPs of MeP (BP1–BP6), along with the proposed reaction pathway of MeP degradation in deionized water. As Lin et al. [36] previously reported the generation of degradation products of methyl-paraben proceeds via three different routes; reaction of MeP molecule with hydroxyl radicals, reaction of MeP with holes photogenerated in TiO₂ and direct oxidation of MeP by oxygen formed by dissolving in water.

Even though degradation mechanisms, similar to those suggested by other studies, are proposed herein, some photocatalytic

intermediates have not been previously reported, indicating that a plethora of BPs may occur depending on the experimental and analytical set up. The structure of most BPs of MeP shows preservation of the core structure of the compound, which can potentially explain the remaining toxicity during the treatment or at least part of it. On the basis of the results presented in this study and also previous studies on the MeP degradation several competing pathways are suggested, in which hydroxylation, dealkylation, methylation, decarboxylation, cleavage of MeP molecule are described as major transformation mechanisms [36,68]. Most of the intermediates identified have aromatic structure but some aliphatic intermediates (BP1 and BP2) have also been detected, which means that ring cleavage occurs at some point of the photocatalytic degradation. In fact, further HO• oxidation caused the cleavage of benzene rings, followed by the generation of low-molecular-weight aliphatic intermediates. The formation of BP1 indicates the cleavage of the MeP ring as a preferential oxidation route, which has been originated from a series of C–C cleavage products such as the formation of methyl acetate. The intermediate BP1 may be attributed to the abstraction of cyclopenta-2,4-dien-1-ol, followed by alkylation on the aliphatic ring and elimination of the hydrogen atoms. Through the photocatalytic treatment, the proposed intermediate of 1,2-dihydroxybenzene is converted into 2,4-hexadienedioic acid (BP2) by the opening of the aromatic ring [36,69]. For this reason, 2,4-hexadienedioic acid can be regarded as the promoter for the formation of an aliphatic by-product BP2 (*m/z* 162).

As shown in Scheme 1 and as previously reported by Lin et al. [36], the 2,4-hexadienedioic acid is oxidized into an aliphatic intermediate (BP2) through some reactions. The hydroxyl radicals attack onto methyl, double bond or benzoic ring, followed by photokolbe reaction which is a decarboxylation of carboxylic acid intermediates via holes. Finally the double bond, is attacked by HO• and O₂ to generate a peroxide intermediate. In turn, this peroxide intermediate transformed into BP2.



Scheme 1. The proposed pathway for the solar-induced heterogeneous photocatalytic degradation of 0.1 g L^{-1} MeP at pH 5.2 and 0.5 g L^{-1} P-25.

As suggested previously, a major reactive specie responsible for the attack on MeP structure are hydroxyl radicals and oxygen dissolved in water which attack the aromatic ring thus leading to the formation of 2,5-dihydroxy-methyl benzoate (**BP4**) and the isomers of 1,4-dihydroxybenzene (**BP3(A)**) or 1,2-dihydroxybenzene (**BP3(B)**) [36,66]; simultaneous abstraction of the $-\text{CH}_3$ group and decarboxylation ($-\text{COOH}$) results in the hydroquinone intermediate (**BP3**) [68]. It is worth mentioning that the isomers **BP3A** or **BP3B** and **BP4** are the most frequently identified oxidation BPs of MeP using various advanced oxidation processes [36,68,69]. Methyl-paraben is attacked by HO^\bullet radicals at $-\text{CH}_3$ and $-\text{H}$ aromatic ring to produce a dihydroxybenzoic acid methyl ester (**BP4**) [36]. This product further oxidized into the phenol, which attacked by HO^\bullet radicals and oxygen dissolved in water, form the isomers of 1,4-dihydroxybenzene (**BP3(A)**) or 1,2-dihydroxybenzene (**BP3(B)**) [69]. These two aromatic compounds are well-known intermediates of the MeP photocatalytic oxidation [36].

The detection of diethyl phthalate (**BP5**) and 1,2-benzenedicarboxylic acid bis-(2-methylpropyl) ester (**BP6**) could be attributed to intramolecular coupling at high concentration [36]. **BP5** and **BP6** can be formed through several reaction mechanisms such as di-hydroxylation and addition of alkyl groups at methyl moiety of MeP. The elucidation routes of the formation **BP5** and **BP6** can be attributed to the di-hydroxylation, addition of 3-methylbutanoic acid group at C-2 of the benzene ring and finally further addition of methyl and isobutene moieties at methyl acetate group, respectively.

3.7. Conclusions

The elimination of methyl paraben, a common antimicrobial was investigated by solar-induced TiO_2 -mediated photocatalysis. The conclusions drawn from this study are summarized as follows:

- (1) The photocatalytic degradation of MeP was completed within 35–45 min under simulated solar irradiation in the presence of Aeroxide TiO_2 P-25 (Evonik) at $0.1\text{--}0.5 \text{ g L}^{-1}$ loading. Other commercial TiO_2 powders that are considered to be active in the visible region of the electromagnetic spectrum, showed remarkably low efficiency after 45 min of treatment, depicting removal percentages as low as 20% (Kronos Vlp 7001) or 40% (Kronos Vlp 7000) at 1 g L^{-1} ; for 100-fold less this amount (i.e. 0.01 g L^{-1}) P-25 reached over 60% MeP elimination.
- (2) The addition of hydrogen peroxide at various concentrations had a detrimental effect on the reaction rate of solar photocatalytic degradation of MeP employing P-25; this is possibly owed to the competitive action of H_2O_2 and dissolved O_2 as electron scavengers, toward the formation of different radical species.
- (3) The inhibiting effect of three radical scavengers, namely 1,4-benzoquinone, potassium iodide and iso-propanol suggests the predominance of $\text{O}_2^{\bullet-}$ as reactive species, whereas hydroxyl radicals followed by photo-generated holes play secondary roles during the solar-induced photocatalytic degradation of MeP with P-25.
- (4) The initial reaction rate of MeP degradation strongly relates to the operating conditions employed, namely, initial solution

pH and substrate concentration. pH₀ becomes important at low MeP concentrations, with higher reaction rates attained at acidic pH rather than neutral or alkaline conditions.

- (5) MeP degradation proceeds with the formation of several hydroxylated aromatic intermediates and two ring-cleavage compounds. Toxicity to *Artemia franciscana* after 24 h of exposure increases during the early stages of the treatment although the original substrate is hardly eco-toxic to the specific test organism at the concentration range in question. The depicted increase in toxicity can be associated to the formation of intermediate compounds that are in turn oxidized.

Acknowledgments

This work was implemented under the REGREW (PE10 (2472)) project within the framework of the Action “Supporting Post-doctoral Researchers” of the Operational Program “Education and Lifelong Learning” (Action’s Beneficiary: General Secretariat for Research and Technology), and is co-financed by the European Social Fund (ESF) and the Greek State. Nireas-International Water Research Center (NEA ΥΠΟΔΟΜΗ/ΣΤΡΑΤΗΓ/0308/09) is co-financed by the Republic of Cyprus and the European Regional Development Fund through the Research Promotion Foundation of Cyprus.

References

- [1] N.A. Liebert, J. Am. Coll. Toxicol. 3 (1984) 147–209.
- [2] N.R. Janjua, G.K. Mortensen, A.M. Andersson, B. Kongshoj, N.E. Skakkebaek, H.C. Wulf, Environ. Sci. Technol. 41 (2007) 5564–5570.
- [3] S.C. Rastogi, A. Schouten, N. de Kruijf, J.W. Weijland, Contact Dermat. 32 (1995) 28–30.
- [4] H.Y. Shen, H.L. Jiang, H.L. Mao, G. Pan, Y.F. Cao, J. Sep. Sci. 30 (2007) 48–54.
- [5] N. Jonkers, A. Sousa, S. Galante-Oliveira, C.M. Barroso, H.-P.E. Kohler, W. Giger, Environ. Sci. Pollut. Res. Int. 17 (2010) 834–843.
- [6] M.G. Soni, I.G. Carabin, G.A. Burdock, Food Chem. Toxicol. 43 (2005) 985–1015.
- [7] E.J. Routledge, J. Parker, J. Odum, J. Ashby, J.P. Sumpter, Toxicol. Appl. Pharmacol. 153 (1998) 12–19.
- [8] S. Oishi, Toxicol. Ind. Health 17 (2001) 31–39.
- [9] P.D. Darbre, A. Aljarrah, W.R. Miller, N.G. Coldham, M.J. Sauer, G.S. Pope, J. Appl. Toxicol. 24 (2004) 5–13.
- [10] S.M. Snedeker, The Ribbon. A Newsletter of the Cornell University Program on Breast Cancer and Environmental Risk Factors (BCERF), vol. 9(1), 2004, pp. 1–2.
- [11] CIR Cosmetic Ingredient Review Expert Panel, Int. J. Toxicol. 27 (Suppl. 4) (2008) 1–82.
- [12] L. Wang, K. Kannan, Environ. Sci. Technol. 59 (2013) 27–32.
- [13] A.G. Asimakopoulou, N.S. Thomaidis, K. Kannan, Sci. Total Environ. 470–471 (2014) 1243–1249.
- [14] T.T. Vo, Y.M. Yoo, K.C. Choi, E.B. Jeung, Reprod. Toxicol. 29 (2010) 306–316.
- [15] H. Yang, T.T. Nguyen, B.S. An, K.C. Choi, E.B. Jeung, Hum. Exp. Toxicol. 31 (2011) 134–144.
- [16] Y. Hu, Z. Zhang, L. Sun, D. Zhu, Q. Liu, J. Jiao, et al., Food Chem. Toxicol. 53 (2013) 69–74.
- [17] K.C. Choi, E.B. Jeung, J. Cell. Mol. Med. 12 (2008) 409–420.
- [18] H.J. Ahn, B.S. An, E.M. Jung, H. Yang, K.C. Choi, E.B. Jeung, Mol. Reprod. Dev. 79 (2012) 626–636.
- [19] Off. J. Eur. Union L342 (2009) 59–209.
- [20] M.G. Kirchhof, G.C. de Gannes, Skin Ther. Lett. 18 (2013) 5–7.
- [21] SCCS Scientific Committee on Consumer Safety, Clarification on opinion SCCS/1348/10 in the light of the Danish clause of safeguard banning the use of parabens in cosmetic products intended for children under three years of age, 2011, pp. 1–51.
- [22] H.B. Lee, T.E. Peart, M.L. Svoboda, J. Chromatogr. A 1094 (2005) 122–129.
- [23] P. Canosa, I. Rodriguez, E. Rubi, M.H. Bollain, R. Cela, J. Chromatogr. A 1124 (2006) 3–10.
- [24] X. Ye, A.M. Bishop, J.A. Reidy, L.L. Needham, A.M. Calafat, Environ. Health Perspect. 114 (2006) 1843–1846.
- [25] N. Jonkers, H.-P.E. Kohler, A. Dammshäuser, W. Giger, Environ. Pollut. 157 (2009) 714–723.
- [26] X. Peng, Y. Yu, C. Tang, J. Tan, Q. Huang, Z. Wang, Sci. Total Environ. 397 (2008) 158–166.
- [27] B. Kasprzyk-Hordern, R.M. Dinsdale, A.J. Guwy, Water Res. 42 (2008) 3498–3518.
- [28] I. González-Mariño, J.B. Quintana, I. Rodríguez, R. Cela, Water Res. 45 (2011) 6770–6780.
- [29] H. Yamamoto, M. Watanabe, S. Katsuki, Y. Nakamura, S. Moriguchi, et al., Environ. Sci. 14 (2007) 97–105.
- [30] D. Błędzka, D. Grylik, J.S. Miller, J. Photochem. Photobiol. A: Chem. 203 (2009) 131–136.
- [31] J. Sánchez-Martín, J. Beltrán-Heredia, J.R. Domínguez, Water Air Soil Pollut. 224 (1483) (2013) 1–12.
- [32] D. Błędzka, M. Gmurek, M. Grylik, M. Olak, J.S. Miller, S. Ledakowicz, Catal. Today 151 (2010) 125–130.
- [33] D. Błędzka, D. Grylik, M. Olak, J.L. Gębicki, J.S. Miller, Radiat. Phys. Chem. 79 (2010) 409–416.
- [34] K.S. Tay, N.A. Rahman, Chemosphere 81 (2010) 1446–1453.
- [35] Y. Lin, C. Ferronato, N. Deng, J.M. Chovelon, Appl. Catal. B: Environ. 104 (2011) 353–360.
- [36] Y. Lin, C. Ferronato, N. Deng, F. Wu, J.M. Chovelon, Appl. Catal. B 88 (2009) 32–41.
- [37] R.J. Steter, R.S. Rocha, D. Dionísio, M.R.V. Lanza, A.J. Motheo, Desalination 272 (2011) 148–153.
- [38] K.L. Willett, R.A. Hites, J. Chem. Educ. 77 (2000) 900–902.
- [39] E.S. Galbavy, K. Ram, C. Anastasio, J. Photochem. Photobiol. Chem. 209 (2010) 186–192.
- [40] T. Miyagi, M. Kamei, T. Mitsuhashi, T. Ishigaki, A. Yamazaki, Chem. Phys. Lett. 390 (2004) 399–402.
- [41] T. Ohno, K. Tokieda, S. Higashida, M. Matsumura, Appl. Catal. A 244 (2) (2003) 383–391.
- [42] A.J. Nozik, in: D.F. Ollis, H. EL-Ekabi (Eds.), Photocatalytic Purification and Treatment of water and Air, Elsevier, Amsterdam, 1993, p. 39.
- [43] F. Méndez-Arriaga, S. Esplugas, J. Giménez, Water Res. 42 (2008) 585–594.
- [44] J.M. Herrmann, Catal. Today 24 (1995) 157–164.
- [45] I.K. Konstantinou, T.A. Albanis, Appl. Catal. B 49 (2004) 1–14.
- [46] A. Fernández, G. Lassaletta, V.M. Jiménez, A. Justo, A.R. González-Elipe, J.M. Herrmann, H. Tahiri, Y. Ait-Ichou, Appl. Catal. B 7 (1995) 49–63.
- [47] J.M. Herrmann, Catal. Today 53 (1999) 115–129.
- [48] Y. Zang, R. Farnood, Top. Catal. 37 (2006) 91–96.
- [49] W. Chu, C.C. Wong, Water Res. 38 (2004) 1037–1043.
- [50] S. Matsuzawa, J. Tanaka, S. Sato, T. Ibusuki, J. Photochem. Photobiol. A 149 (2002) 183–189.
- [51] P. Pichat, C. Guillard, L. Amalric, A.C. Renard, O. Plaidy, Sol. Energy Mater. Sol. Cells 38 (1995) 391–399.
- [52] B. Neppolian, H.C. Choi, S. Sakthivel, B. Arabindoo, V. Murugesan, Chemosphere 46 (2002) 1173–1181.
- [53] D.D. Dionysiou, M.T. Suidan, I. Baudin, J.M. Lainé, Appl. Catal. B 50 (2004) 259–269.
- [54] T. Hirakawa, Y. Nosaka, Langmuir 18 (2002) 3247–3254.
- [55] M.W. Peterson, J.A. Tumer, A.J. Nozik, J. Phys. Chem. 95 (1991) 221–225.
- [56] L.A. Ioannou, E. Hapeshi, M.I. Vasquez, D. Mantzavinos, D. Fatta-Kassinos, Sol. Energy 85 (2011) 1915–1926.
- [57] L.M. Yang, L.E. Yu, M.B. Ray, Environ. Sci. Technol. 43 (2009) 460–465.
- [58] X. Van Doorslaer, P.M. Heynderickx, K. Demeestere, K. Debevere, H. Van Langenhove, J. Dewulf, Appl. Catal. B 111–112 (2012) 150–156.
- [59] Q.Z. Zhang, X.H. Qu, H. Wang, F. Xu, X.Y. Shi, W.X. Wang, Environ. Sci. Technol. 43 (11) (2009) 4105–4112.
- [60] P. Salvador, J. Phys. Chem. C 111 (2007) 17038–17043.
- [61] A. Zacharakis, E. Chatzizymeon, V. Binas, Z. Frontistis, D. Venieri, D. Mantzavinos, Int. J. Photoenergy (2013), 9 pp., Article ID 570587.
- [62] L. Yang, L.E. Yu, M.B. Ray, Water Res. 42 (2008) 3480–3488.
- [63] J. Chen, L. Eberlein, C.H. Langford, J. Photochem. Photobiol. A: Chem. 148 (2002) 183–189.
- [64] F. Kiriakidou, D.I. Kondarides, X.E. Verykios, Catal. Today 54 (1999) 119–130.
- [65] H. Lachheb, E. Puzenat, A. Houas, M. Ksibi, E. Elaloui, C. Guillard, J.M. Herrmann, Appl. Catal. B 39 (2002) 75–90.
- [66] M. Terasaki, M. Makino, N. Tatarazako, J. Appl. Toxicol. 29 (2009) 242–247.
- [67] I. Bazin, A. Gadal, E. Touraud, B. Roig, in: D. Fatta-Kassinos, K. Bester, K. Kümmerer (Eds.), Xenobiotics in the Urbanwater Cycle: Mass Flows, Environmental Processes, Mitigation and Treatment Strategies. Environmental Pollution, Springer, 2010, pp. 245–257.
- [68] X. Feng, Y. Chen, Y. Fang, X. Wang, Z. Wang, T. Tao, Y. Zuo, Sci. Total Environ. 472 (2014) 130–136.
- [69] S. Chatterjee, A. Sakar, S.N. Bhattacharyya, J. Photochem. Photobiol. A: Chem. 81 (1994) 199–203.